J|A|C|S
ARTICLES
Published on Web 04/06/2002

Photocurrent Generation in Multilayer Organic−Inorganic Thin Films with Cascade Energy Architectures

Feras B. Abdelrazzaq, Raymond C. Kwong, and Mark E. Thompson*

Contribution from the Department of Chemistry, University of Southern California, Los Angeles, California 90089

Received July 12, 2001

Abstract: Zirconium organobisphosphonate multilayer thin films of viologen derivatives were grown on copper dithiolate multilayers of 5,15-di(*p*-thiolphenyl)-10,20-di(*p*-tolyl)porphyrin (POR) and 5,15-di(*p*-thiolphenyl)-10,20-di(*p*-tolyl)porphyrinzinc (ZOR) on a variety of substrates (e.g. Au, SiO_2), using solution depositions methods. The multilayer structures were studied by atomic force microscopy, UV−vis spectroscopy, and ellipsometry. In the case of copper dithiolate thin films, layer-by-layer lamellar growth with low surface roughness resulted, while higher surface roughness was observed in the growth of Zr viologen bisphosphonate films. Gold electrodes modified with zirconium bisphosphonate multilayers of viologen on top of copper dithiolate multilayers of porphyrin derivatives (ZOR or POR) were photoelectroactive and produced efficient and stable photocurrents using visible light. By arranging the zinc-porphyrin (ZOR) and the free base porphyrin (POR) donors in an energetically favorable fashion, according to their redox potentials and optical energy gaps, the photoinduced charge separation was improved, and higher photocurrent quantum yields (∼4%) and fill factor (∼50%) of the photoelectrode were achieved.

Introduction

Mimicking the photosynthetic process is one of the most important goals in modern chemistry. The aim is to construct an artificial system that mimics the overall energy transformation process in natural photosynthesis, in which photoinduced charge separation leads to reduction and oxidation reactions, effectively converting optical energy into chemical potential.[1−3] Systematic organization of photon harvesting groups, electron donors, and electron acceptors on the molecular level is the basis of efficient photoinduced charge separation, with minimum back electron transfer.[1,4−7] The construction of molecular systems, with redox components arranged at fixed distances by covalent bonding, has been extensively studied.[6−8] Charge separation rates of well-designed donor−acceptor pairs in these molecular systems can be very high; however, the charge recombination rate is often very high as well. This results in low charge separation quantum yields and leaves the charge-separated state extremely short-lived (picosecond or less).[5]

A great deal of work was devoted to develop supramolecules that mimic the stepwise nature of photosynthetic charge separation, which involves initial charge separation followed by a sequence of dark electron transfer processes that proceed at rates sufficiently fast to compete with the back electron-transfer processes. The sequence of dark electron-transfer reactions facilitates spatial charge separation of the hole and electron after the initial charge separation, resulting in lower charge recombination yields.[5] A good example of such a multistep electron-transfer system has been reported by Gust et al.[6,9] for a carotene-Zn porphyrin-free base porphyrin-naphthoquinone-benzoquinone (C-P_{Zn}-P-Q_a-Q_b) pentad. In this system, the carotene-Zn porphyrin-free base porphyrin donors were organized according to their redox potentials and optical energy gaps, in a manner that favors exciton migration to the donor−acceptor (D−A) interface and introduces a gradient of chemical potential (HOMO energies) that draws the hole away from the D−A interface (a cascade arrangement) to the carotene. The acceptors Q_a and Q_b are similarly cascaded, drawing the

* To whom correspondence should be addressed. E-mail: met@usc.edu. Phone: (213)740-6402. Fax: (213)740-8594.

(1) Keller, S.; Johnson, S.; Brigham, S.; Yonemoto, E.; Mallouk, T. *J. Am. Chem. Soc.* **1995**, *117*, 12879. Chouldhury, B.; Weedon, A.; Bolton, J. *Langmuir* **1998**, *14*, 6199.
(2) (a) Shah, A.; Torres, P.; Tscharner, R.; Wyrsch, N.; Keppner, H. *Science* **1999**, *285*, 692. (b) Byrd, H.; Suponeva, E.; Bocarsly, A.; Thompson, M. *Nature* **1996**, *380*, 610. (c) Vermeulen L.; Snover J.; Sapochak L.; Thompson M. *J. Am. Chem. Soc.* **1994**, *116*, 3175.
(3) Lewis, N. S. *Am. Sci.* **1995**, *83*, 534−541.
(4) Uosaki, K.; Kondo, T.; Zhang, X.; Yanagida, M. *J. Am. Chem. Soc.* **1997**, *119*, 8367.
(5) Wasielesky, M. *Chem. Rev.* **1992**, *92*, 435.
(6) Gust, D.; Moore, T.; Moore, A.; Macpherson, A.; Lopez, A.; DeGraziano, A.; Gouni., I.; Bittersman, E.; Seely, G.; Gao, F.; Nieman, R.; Ma, X.; Demanche, L.; Hung, S.; Luttrull, D.; Kerrigan, P. *J. Am. Chem. Soc.* **1993**, *115*, *11141*.
(7) (a) Durantini, E.; Moore, A.; Moore, T.; Gust, D. *Molecules* **2000**, *5* (3), 529. (b) Krasnovsky, A.; Bashtanov, M.; Drozdova, N.; Liddell, P.; Moore, A.; Moore, T.; Gust, D. *J. Photochem. Photobiol. A* **1997**, *102*, 157. (c) Macpherson, A.; Liddell. P.; Lin, S.; Noss, L.; Seely, G.; Dergraziano, J.; Moore, A.; Moore, T.; Gust, D. *J. Am. Chem. Soc.* **1995**, *117*, 7202.
(8) (a) Wasielewski, M. R.; O'Neil, M.; Gosztola, D.; Niemczyk, M.; Svec, W. *Pure Appl. Chem.* **1992**, *64*, 1319−1325. (b) Wasielewski, M. R. *Chem. Rev.* **1992**, *92*, 435. (c) Wasielewski, M. R.; Gaines, G.; Wiederrecht, G.; Svec, W.; Niemczyk, M. *J. Am. Chem. Soc.* **1993**, *115*, 10442−10443. (d) Hasharoni, K.; Levanon, H.; Greenfield, S.; Gasztola, D.; Svec, W.; Wasielewski, M. R. *J. Am. Chem. Soc.* **1995**, *117*, 8055−8056. (e) Wiederrecht, G.; Niemczyk, M.; Svec, W.; Wasielewski, M. R. *J. Am. Chem. Soc.* **1996**, *118*, 81−88. (f) Greenfield, S.; Svec, W.; Gasztola, D.; Wasielewski, M. R. *J. Am. Chem. Soc.* **1996**, *118*, 6767−6777.
(9) Gust, D.; Moore, T.; Moore, A.; Lee, S.; Bittersman, E.; Luttrull, D.; Rehms, A.; DeGraziano, A.; Ma, X.; Gao, F.; Belford, R.; Trier, T. *Science* **1990**, *248*, 199.

10.1021/ja011700m CCC: $22.00

electron away from the D−A interface. This cascade arrangement results in an overall increase of photoinduced charge separation quantum yields and lifetime of the resulting ion pair. Excitation of the porphyrins of C-P_{Zn}-P-Q_a-Q_b resulted in the formation of the charge-separated state ($C^{\bullet+}$-P_{Zn}-P-Q_a-$Q_b^{\bullet-}$), with a quantum yield of 0.60 and a lifetime of 200 μs.

To extract the energy of a charge-separated state in a usable fashion, efforts have been devoted to spatially organize the redox components on solid supports,[10] such as lipid bilayer membranes,[11] sol−gel glasses,[12] polyelectrolytes,[1] and semiconductor nanocrystallites modified with a photosensitizer dye.[13] Organization of the redox components on solid supports has resulted in high quantum yields and longer lifetimes of the photoinduced charge-separated states relative to those in solution.

Langmuir− Blodgett[14] and self-assembly [2,4,15,16] techniques have been successfully used to organize photoactive molecules into highly ordered macroscopic structures. Using self-assembly methods, it was possible to organize molecular redox components in a stable lamellar structure at various solid supports. This resulted in an efficient artificial photosynthetic system that combined the advantages of molecular systems with those of solid-supported systems.[17]

We recently reported photocurrent generation from a photoelectrode made from Zr phosphonate multilayers of phenylenediamine (electron donor) and viologen (electron acceptor).[2] This device produced a stable and repeatable photocurrent upon irradiation of light in the 250−350 nm region. Here we describe the construction and characterization of multilayer assemblies made from copper dithiolate multilayer films composed of porphyrin derivatives, which act as electron-donor layers, and zirconium bisphosphonate multilayer films composed of a viologen derivative, which act as electron-acceptor layers.

Scheme 1

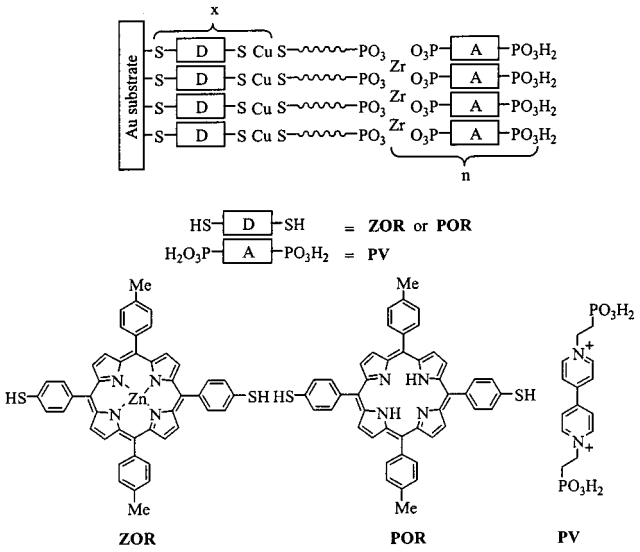

Scheme 1 depicts the structure of the porphyrins and the viologen derivative that were synthesized and studied. The porphyrin moieties have a strong absorption in the visible spectrum, which ensures high optical density for the photoelectrode. We have found that by assembling the porphyrin derivatives spatially, according to their redox potentials and optical energy gaps, the photoinduced charge-separation yields improved, hence improving the quantum yields and the photoelectrochemical behavior of the device.

Results and Discussion

In designing the heterolamellar structure used here, it is important to know the relevant energy levels of the HOMO and LUMO of the donors and acceptors. UV−vis absorption and emission spectroscopies as well as cyclic voltammetry were used to study the photophysical and electrochemical characteristics of the derivatives described here, allowing the estimation of their relative HOMO and LUMO energies. The photophysical properties of PV were reported previously.[15] PV has a broad absorption band in the ultraviolet (λ_{max} = 270 nm) and similar absorption characteristics were observed in Zr-bisphosphonate films of PV. Figure 1 shows the absorption spectra of ZOR and POR in CH_2Cl_2 solution. The POR absorption spectrum in solution exhibits a strong Soret band with λ_{max} = 420 nm and four Q-bands at λ_{max} = 516, 552, 592, and 648 nm. The ZOR absorption spectrum in solution has a similar Soret band (λ_{max} = 424 nm) and two Q-bands at λ_{max} = 550 and 588 nm. The red shift and the decrease in the number of Q-bands seen in ZOR relative to POR is commonly observed in comparing free base porphyrins to their Zn-substituted analogues.[4,18] From the intersection of the absorption Q-band and emission bands in solution, the optical energy gaps were estimated to be 1.91 and 2.08 eV for POR and ZOR, respectively (see arrows in Figure 1).

Cyclic voltammetry of viologen-bisphosphonate (PV) shows a reversible one-electron reduction at E° = −0.67 V vs SCE in aqueous solution, which is typical for dialkyl viologen derivatives.[15] POR shows reversible oxidations at 1.0 and 1.3 V vs SCE, which is typical for porphyrin oxidations.[4] ZOR shows

(10) (a) Borja, M.; Dutta, P. *Nature* **1993**, *362*, 43. (b) Yonemoto, E.; Kim, H.; Schmehl, R.; Wallin, J.; Shoulders, B.; Richardson, B.; Haw, J.; Mallouk, T. *J. Am. Chem. Soc.* **1994**, *116*, 10557
(11) (a) Seta, P.; Bienvenue, E.; Moore, A.; Mathis, P.; Bensasson, R.; Liddell, P.; Pessiki, P.; Joy, A.; Moore, T. *Nature* **1985**, *316*, 653. (b) Sakata, Y.; Tatemitsu, H.; Bienvenue, E.; Seta, P. *Chem. Lett.* **1988**, 1625−1628.
(12) (a) Slama-Schwok, A.; Avnir, D.; Ottolenghi, M. *Nature* **1992**, *355*, 240. (b) Sassoon, R.; Gershuni, S.; Rabani, J. *J. Phys. Chem.* **1992**, *96*, 4692.
(13) (a) Naser, C.; Hotchandan, S.; Kamat, P. *J. Phys. Chem. B* **1998**, *102*, 4944. (b) Nazeeruddin, M. K.; Kay, A.; Rodici, I.; Humphry, B.; Mueller, E.; Liska, P.; Valchopoulos, N.; Graetzel, M. *J. Am. Chem. Soc.* **1993**, *115*, 6382. (c) Hagefldt, A.; Gratzel, M. *Acc. Chem. Res.* **2000**, *33*, 269. (d) Krishnan, M.; Zhang, X.; Bard, A. *J. Am. Chem. Soc.* **1984**, *106*, 7371. (e) Debestani, R.; Bard, A.; Campion, A.; Fox, M.; Mallouk, T.; Webber, S.; White, J. *J. Phys. Chem.* **1988**, *92*, 1872. (f) Kim, Y.; Atheron, S.; Brigham, E.; Mallouk, T. *J. Phys. Chem.* **1993**, *97*, 11802.
(14) (a) Fujihira, M.; Sakomura, M. *Thin Solid Films* **1989**, *179*, 471. (b) Sakomura, M.; Fujihira, M. *Thin Solid Films* **1996**, *273*, 181.
(15) Snover, J.; Byrd, H.; Suponeva, E.; Vicenzi, E.; Thompson, M. *Chem. Mater.* **1996**, *8*, 1490.
(16) (a)Vermuelen, L.; Thompson, M. *Chem. Mater.* **1994**, *6*, 77. (b) Vermuelen, L.; Snover, J.; Sapochak, L.; Thompson, M. *J. Am. Chem. Soc.* **1993**, *115*, 11767. (c) Vermuelen, L.; Thompson, M. *Nature* **1992**, *358*, 656. (d) Ungashe, S.; Wilson, W.; Katz, E.; Scheller, G.; Putvinski, T. *J. Am. Chem. Soc.* **1992**, *114*, 8717. (e) Ulman, A. *Introduction to Ultrathin Organics Films: From Langmiur-Blodgett to Self-assembly*; Academic Press: Boston, 1991. (f) Laibinis, P.; Whitesides, G.; Allara, D.; Tao, Y.; Parikh, A.; Nuzzo, R. *J. Am. Chem. Soc.* **1991**, *113*, 7152. (g) Laibinis, P.; Whitesides, G. *J. Am. Chem. Soc.* **1992**, *114*, 1990. (h) Finkles, H.; Avery, S.; Lynch, M.; Furtsch, T. *Langmiur* **1987**, *3*, 409. (i) Thompson, M. *Chem Mater.* **1994**, *6*, 1168. (j) Widrig, C. A.; Chung, C.; Porter, M. D. *J. Electroanal. Chem.* **1991**, *310*, 335. (k) Tao, Y.-T.; Wu, C.-C.; Eu, J.-Y.; Lin, W.-L. *Langmuir* **1997**, *13*, 4018. (l) Kondo, T.; Ito, T.; Nomura, S.; Uosaki, K. *Thin Solid Films* **1996**, *284/285*, 652. (m) Kondo, T.; Yanagida, M.; Nomura, S.; Ito, T.; Uosaki, K. *J. Electroanal. Chem.* **1997**, *438* (1−2), 121. (n) Akiyama, T.; Imahori, H.; Ajawakom, A.; Sakata, Y. *Chem. Lett.* **1996**, 907. (o) Fujihira, M. *Mol. Cryst. Liq. Cryst.* **1990**, *183*, 59.
(17) (a)Alberti, G.; Constantino, U.; Alluhi, S.; Tomassini, N. *Inorg. Nucl. Chem.* **1978**, *40*, 1113. (b) Gao, G.; Hong, H.; Mallouk, T. *Acc. Chem. Res.* **1992**, *25*, 420. (c) Katz, E. *Chem. Mater.* **1994**, *6*, 2227. (d) Clearfield, A. *Comments Inorg. Chem.* **1990**, *10*, 89. (e) Thompson, M. *Chem. Mater.* **1994**, *6*, 1168.

(18) Sessler, J.; Jonson, M.; Lin, I. *Tetrahedron* **1989**, *45*, 4767.

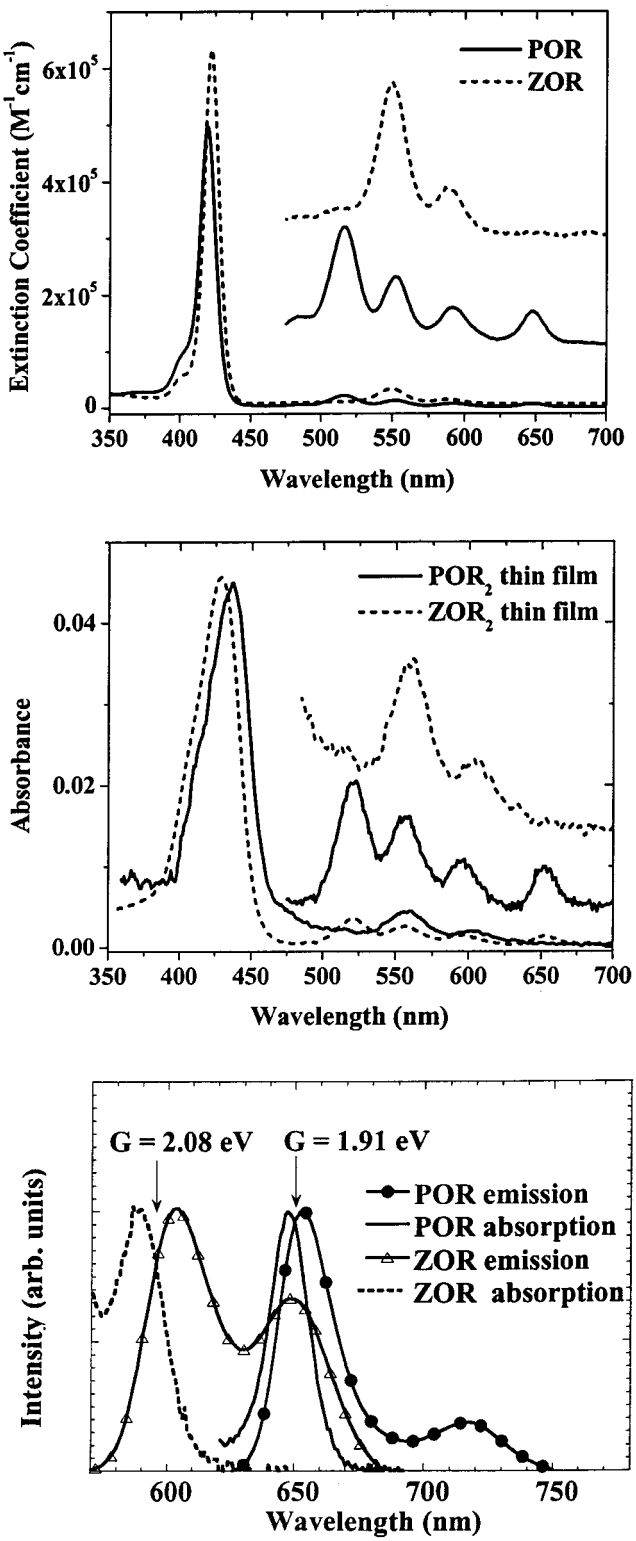

Figure 1. (Top) Solution absorption spectrum of ZOR (- - -) and POR (solid line) in CH_2Cl_2. The inset spectra have been amplified by a factor of 10 and offset for clarity. (Middle) Absorption spectra of POR and ZOR thin films. The inset spectra have been amplified by a factor of 5 and offset for clarity. (Bottom) Estimations of the energy gaps have been based on the intersection of the Q-band absorption and emission spectra of POR and ZOR in CH_2Cl_2 at room temperature. The energy gaps (G) are estimated to be 1.91 and 2.08 eV for POR and ZOR, respectively.

reversible oxidations at 0.88 and 1.16 V vs SCE. From the first oxidation potential for POR and ZOR and their HOMO-LUMO gaps (approximated by the optical energy gaps), LUMO energy levels are estimated to be −0.91 and −1.20 V (vs SCE) for POR and ZOR, respectively.

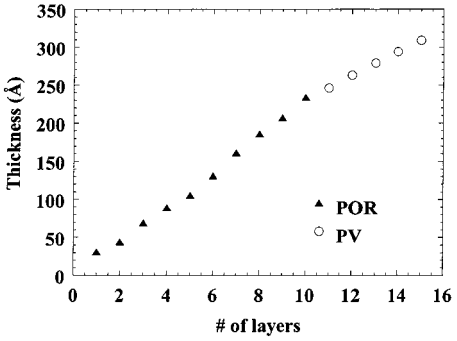

Figure 2. Thickness as a function of layers for the CuPOR (triangle) film followed by ZrPV (circle). Best fit of the growth gives a slope of 23 Å for POR and 16 Å for PV.

Film Growth and Characterization. Layer-by-layer deposition was carried out by sequential treatment of the substrate with solutions of a metal salt (Cu^{2+} or Zr^{4+}) and the appropriate difunctional organic group. To initiate the growth of the Cu-thiolate films on gold surfaces, the substrate surface was functionalized with thiol groups by adsorption of a monolayer of porphyrin dithiolate (ZOR or POR). To prevent the oxidative oligomerization of the porphyrin molecules (via formation of disulfide linkages), the dithiol solution was thoroughly purged with nitrogen and the deposition was carried out under positive pressure of nitrogen. For quartz substrates, 3-mercaptopropyltriethoxysilane was used to form a thiol-rich surface. Cu-thiolate films were then grown by alternative treatment of the substrate with Cu(II) acetate (10 min) and the dithiol solutions (20 min).

The advantage of the self-assembly method reported here is the ease of adding one type of multilayer thin film on top of another. To change the multilayer films from one porphyrin derivative to another, the dithiolate solutions are changed in successive growth steps. The chemistry used to grow the self-assembled layers can also be readily changed during the multilayer growth process. To build multilayers of Zr-bisphosphonate on top of Cu-thiolate films, a difunctional molecule that has a thiol group on one side and a phosphonic acid group on another (e.g., mercaptobutylphosphonic acid) was used as a transitional molecule between the two films. Binding the thiol side of the molecule to the Cu-rich surface leaves phosphonic acid groups on the surface and makes the surface suitable for growth of Zr phosphonate films. The Zr-bisphosphonate films were grown by alternative treatment of the $ZrOCl_2$ (15 min) and viologen-bisphosphonates (20 min) at 70 °C.

The growth of Cu-porphyrin-dithiolates was monitored by UV−vis spectroscopy and by ellipsometry. Electronic spectra of the Cu-thiolate films of porphyrin derivatives POR and ZOR grown on quartz substrate show linear incremental increase of absorption as a function of the number of deposition cycles. The growth of Zr-bisphosphonates of various chromophores has been studied in detail.[15,17] Electronic spectra of the Zr-viologen-bisphosphonate films grown on quartz show a linear increase of absorption as a function of the number of deposition cycles. The linear increase in absorbance vs number of depositions in these multilayer films indicates that the same amount of a given material is added to the substrate with each deposition cycle, but does not verify uniformity of the layer's growth.[15] Figure 2 shows ellipsometric data of the growth of Cu-thiolate films of

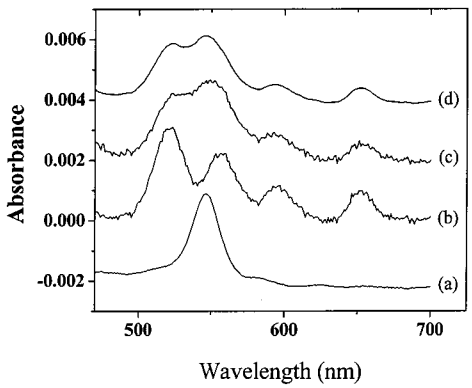

Figure 3. Absorption spectra of solution and thin films samples: (a) the solution spectrum of copper(II)-5,10,15,20-tetraphenylporphyrin (CuTPP, CH_2Cl_2 solvent); (b) a self-assembled monolayer of POR deposited on glass; (c) the POR monolayer film after 15 min of exposure to a solution of $Cu(OAc)_2$; and (d) the result of summing the POR and CuTPP solution spectra (1:1 ratio). The concentrations of the two solutions (Figure 1, top, and part a of this figure, respectively) are roughly equal.

porphyrin derivatives on gold followed by the growth of five layers of Zr-viologen-bisphosphonate. These data show a linear incremental increase of thickness with each deposition cycle of both Cu-porphyrin-dithiolate film and Zr-viologen-bisphosphonate film. Ellipsometric thickness measured at various points on the substrate surface shows very little deviation, as expected for a uniform thin film. The slope of the ellipsometric growth on gold gives a layer thickness of 23 Å/layer for Cu-thiolate of porphyrin. Molecular modeling of POR minimizes to a structure with 19 Å between S atoms. Molecular modeling of POR was carried out with *CS Chem 3D Pro*, using an MM2 force field (CambridgeSoft Corporation, Cambridge, MA). The 4 Å difference agrees with the expected lengths of the Cu−thiolate linkages. This analysis suggests that these molecules form multilayers with the molecular axis perpendicular to the gold surface.

Atomic force microscopy (AFM) was employed to investigate the surface morphology of these multilayer films. Films that are uniform and fully assembled should reveal smooth surfaces by AFM, and those that are not uniform and are not complete should have rough surfaces. When grown on a polished silicon surface (rms roughness is 2 Å), Zr-bisphosphonate multilayers give surfaces with low rms roughness, ca. 10−20 Å, as an indication of their lamellar growth. However, in the case of Zr-viologen-bisphosphonate multilayers microcrystalline domains were observed on the surface and their AFM measurements revealed large bumps which resulted in very high rms roughness (200 Å for eight layers of ZrPV).[15] In the case of Cu-dithiolate multilayers, smooth surfaces are observed. When grown on gold substrate (rms roughness 13−14 Å), a five-layer film of POR (110 Å thick) produced a surface with rms roughness of 23 Å. The observed low surface roughness indicates tightly packed lamellar film growth of these films. A film consisting of three POR followed by three ZrPV layers gave an rms roughness of 39 Å. The large increase of surface roughness upon addition of only three Zr-viologen-biphosphonate layers to the POR film indicates that viologen-bisphosphonate multilayers are most likely not growing in a well-controlled lamellar fashion. A similar nonlamellar growth pattern was observed previously for the growth of these films on other surfaces. In our device assembly, we utilize viologen as an electron relay from the porphyrin layers to the solution. Thus, few layers of Zr-viologen-bisphosphonates are needed on the top of the donor layers (Cu-thiolate films). This excludes many of the pinholes that may form from their nonuniform growth.

UV−vis spectra of Cu-thiolate films of POR and ZOR on quartz show a 8−10 nm red-shift and an increased line width of the Soret bands relative to those in solution, suggesting the presence of an electronic interaction between the porphyrin rings in the self-assembled films (see Figure 1 (top and middle)).[4,16d,19] From the optical densities of the films and the measured extinction coefficients for the porphyrin moieties, we estimated the surface coverage to be 5×10^{13} moleculse/cm^2. The coverage here is less than that seen for tetraarylporphyrin monolayers prepared by Langmuir−Blodget and self-assembly techniques (porphyrin-thiols on gold substrates), which can give coverages as high as 7×10^{13} molecules/cm^2.[4,20] We attribute the lower coverage here to incomplete silation of the glass surface.

The Q-bands of the ZOR films closely match the solution spectrum of ZOR, while the POR films are slightly different (Figure 1 (middle)). The POR bilayer of Figure 1 shows an enhanced band at 550 nm, relative to the POR solution spectrum of Figure 1. The Q-band spectrum for a single layer of POR matches the POR solution spectrum more closely (Figure 3b). This POR film has not been exposed to free Cu ions in solution. When the POR layer is treated with a solution of $Cu(OAc)_2$, as part of the multilayer growth step, the spectrum shows a marked enhancement of the 550 nm band, Figure 3c. This increased intensity at 550 nm suggests that partial metalation of the POR ligands by Cu^{2+} has taken place. The spectrum of copper-tetraphenylporphine (CuTPP) gives its λ_{max} near 550 nm, Figure 3a. If equal amounts of the POR and CuTPP spectra are summed (1:1 ratio), the resulting spectrum matches the observed Cu treated POR spectrum closely (Figure 3d). On the basis of this analysis we expect that the POR film on glass is roughly 50% metalated during the growth process on SiO_2. The POR_2 film does not show as high a level of metalation, because only one of the POR layers has been exposed to free Cu^{2+} ions.

Unfortunately, we cannot use electronic spectroscopy to probe our thin films on gold substrates (the system used for the photovoltaic experiments). To examine the metalation of POR during film growth on gold, the electrochemistry of a monolayer of POR grown on gold was examined, before and after treatment with $Cu(OAc)_2$ solution. The two films (POR and Cu^{2+} treated POR) give identical cyclicvoltametric scans, with oxidation potentials close to that of POR in solution. For comparison, a monolayer was grown from a solution containing both POR and $Cu(OAc)_2$. The POR readily metalates in this solution, prior to deposition, leading to a monolayer of the copper-POR complex. This Cu-metalated POR monolayer film has an oxidation potential that is 0.35 V less than the potentials observed for the POR films, and is not observed in the electrochemistry of the POR films. These experiments indicate that the POR films grown on gold substrates have very low levels of Cu metalation during the film growth, in contrast to the behavior seen for POR films on SiO_2 substrates. The principal difference between the films grown on the two

(19) Zak, J.; Yuan, H.; Ho, M.; Woo, L.; Porter, M. *Langmuir* **1993**, *9*, 2772.
(20) Van Galen, D.; Majda, M. *Anal. Chem.* **1988**, *60*, 1549.

substrates is the packing density of the porphyrin monolayer. Monolayers grown from thiol-derivatized prophyrins on gold substrates, very similar to those used here, give higher packing densities than we observed for our films on glass.[4,20] The higher packing density for the POR films on gold substrates, relative to those grown on SiO_2, may retard the diffusion of copper ions into the film, preventing significant metalation of the POR during the 15 min treatment of the film with $Cu(OAc)_2$, used in film growth.

Exchange of Zn^{2+} ions of ZOR for Cu^{2+} ions in solution is not observed. Treatment of thin-film samples of ZOR or free ZOR in solution with $Cu(OAc)_2$ does not lead to observable levels of CuPOR, under our experimental growth conditions (exchange monitored by absorption and fluorescence spectroscopies). On the basis of spectroscopic and electrochemical measurements we expect that the POR and ZOR films on gold substrates have low CuPOR impurity levels.

Photocurrent Generation. The first photochemical experiment was conducted by immersing a gold electrode modified with 3 layers of POR followed by three layers of PV (POR_3/PV_3 electrode) in a 0.1 M solution of $LiClO_4$. A schematic diagram of the multilayers studied is shown in Scheme 1. Irradiation of the photoelectrodes under aerobic conditions leads to a small unstable photocurrent. Addition of PV (Scheme 1) in solution (0.025 M) led to a stable cathodic photocurrent that decayed instantly when illumination was stopped. Similar behavior was observed with use of dimethyl viologen in place of PV. Viologen was chosen as the electron relay because the electron-transfer rate of this group is known to be fast.[21] The photoelectrode can be repeatedly cycled, giving the same photocurrent.

Measurements of photocurrent were carried out by holding the potential of the photoelectrode (working electrode) at 0 V versus a standard calomel electrode (SCE). The polarity of the photocurrent indicates that the electrons were photochemically promoted from the porphyrin donor to the viologen acceptor in the film then passed to PV in solution. Charge separation at a porphyrin/viologen interface of this type has been reported previously. Katz et al. reported efficient electron-transfer quenching of the POR excited state by viologen in an adjacent layer, separated by a zirconium−phosphonate layer.[16d] The principal difference between the porphyrin/viologen interface in our system and that of Katz is the insertion of a mercaptobutylphosphonic acid group between the POR donor and VIOL acceptor layers in the films reported here. The mercaptophosphonic acid is required as a transition between the copper-sulfide and zirconium-phosphonate growth systems. If the butyl group is fully chain extended and the multilayer films were highly ordered, the donor−acceptor separation will be roughly 6 Å longer than that of Katz's films. This increase in donor−acceptor separation would be expected to severely decrease the photoinduced electron transfer. On the basis of the AFM studies of the POR_3/PV_3 films (POR layers have rms roughness of 13−14 Å), we expect that the interface between the POR and PV layers is not as well ordered as suggested by the ellipsometric data (Figure 2) or as pictured in Scheme 1. Charge separation could be occurring at regions where the interfacial layer is less ordered and the POR/viologen distance could be similar to that of Katz's film.

(21) Reis, K.; Joshi, V.; Thompson, M. *J. Catal.* **1996**, *161*, 62.

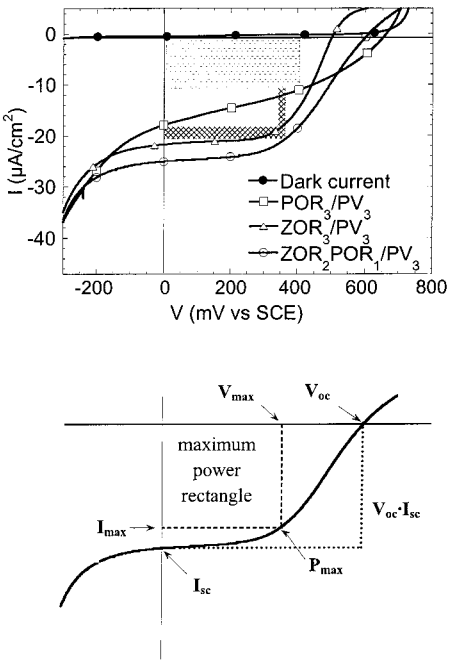

Figure 4. (top) Current−voltage curves produced by Au·POR_3/PV_3, Au·ZOR_3/PV_3, and Au·ZOR_2POR_1/PV_3 electrodes under illumination and a representative dark current produced by the Au·ZOR_2POR_1/PV_3 electrode. The electrodes were immersed in a 2×10^{-2} M aqueous solution of PV. The potential of the working electrode was set at 0 V vs SCE. The photolysis was carried out using white light through a filter that passed only wavelengths greater than 390 nm (13.32 mW cm^{-2} for wavelengths of 390−540 nm). The MPR of each electrode is represented by the patterned rectangle. (Bottom) Description of short-circuit current, I_{sc}, open-circuit voltage, V_{oc}, and maximum power rectangle of the Au·ZOR_2POR_1/PV_3 electrode.

A ZOR_3/PV_3-modified electrode gave a stable photocurrent, with the same polarity as observed for the POR_3/PV_3 electrode. Figure 4 shows the current−voltage (IV) characteristics of POR_3/PV_3 and ZOR_3/PV_3 modified gold electrodes in the dark and when illuminated with white light. The UV portion of the white light was removed with a 390 nm cutoff filter leaving a maximum intensity of 13.32 mW cm^{-2} for the 390−540 nm region of the spectrum. An important feature in the device assemblies reported here is the small dark current observed (0.4 $\mu A/cm^2$ at short circuit) relative to a naked electrode (21.4 $\mu A/cm^2$ at the short circuit), which is a good indication of the uniformity and efficient coverage of the surface by the multilayer assemblies, i.e. very few pinholes or cracks are present in the multilayer films.

When the POR or ZOR electrodes were illuminated at 0 V versus SCE, the short circuit current densities were 18 and 21 $\mu A\ cm^{-2}$ and the calculated quantum yields (current/absorbed photons) were 2.4 and 2.3% for POR_3/PV_3 and ZOR_3/PV_3 electrodes, respectively. Quantum yields, based on the number of photons adsorbed by the film, were calculated by using short circuit current (I_{sc}) 0 V vs SCE and the absorbance determined from the absorbance spectrum of identical multilayer films grown on quartz substrates. The measured optical density of a three-layer film of ZOR (λ_{max} 434 nm) on quartz is 0.14, while a three-layer film of POR gives an optical density of 0.11 (λ_{max} 430 nm). The calculated power absorbed by the porphyrin moieties was 2.1 and 2.5 $\mu W\ cm^{-2}$ for POR_3/PV_3 and ZOR_3/PV_3 modified quartz substrate, respectively. From the I−V characteristics, the fill factor (ff) of these devices can be

evaluated. The fill factor is defined as the maximum power rectangle that can be drawn inside the I−V performance curve of the device divided by the area of the rectangle bounded by V_{oc}·I_{sc} (Figure 4). The photovoltages at the open circuit (V_{oc}) were 660 and 500 mV (vs SCE) and the calculated fill factors were 37 and 58% for POR_3/PV_3 and ZOR_3/PV_3 electrodes, respectively. The maximum power rectangles were calculated (see Figure 4) for the two electrodes to be 4.3 and 6.3 μW cm^{-2}, respectively. The photoenergy conversion efficiencies (output electrical watt/incident optical watt) were calculated to be 0.04 and 0.05%, respectively. The photoenergy conversion efficiency was calculated by dividing the maximum power rectangle obtained from the I−V performance of the device over the power of incident light at an intensity of 13.32 mW/cm^2. The overall improvement of the fill factor and the photovoltaic performance observed in ZOR_3/PV_3 relative to POR_3/PV_3 suggests that there is a more efficient charge separation in the former, which may be the result of a higher rate of initial charge separation for ZOR/PV relative to POR/PV.

The photocurrent behavior observed for both electrodes is a significant improvement over that of the earlier reported electrode assembled from films of ZrPV and Zr phenylenediamine bisphosphonate (PAPD) donor films.[2a] The porphyrin derivatives offer the advantage of strong absorption in the visible region relative to phenylenediamine (PAPD), which is active in the UV region (250−300 nm). The reported best performance was for the $PAPD_2/PV_2$ electrode. Photolysis of the $PAPD_2/PV_2$ electrode with white light (14 mW cm^{-2} in the active region of the device) resulted in low open circuit voltages (112 mV) and a small photocurrent (3.1 μA cm^{-2}). Thin film devices similar to those described here have been reported, and consist of photoelectroactive materials (i.e., cyanine dyes, chlorophyll *a*, chlorophyll *b*) assembled on optically transparent metal oxide electrodes (i.e., SnO_2, Sb-doped SnO_2, indium−tin oxide) by Langmuir−Blodgett or film casting techniques.[22] The ZOR- and POR-based photoelectrodes reported here have significantly higher fill factors and open circuit voltages than those reported for these related thin-film devices.[22] The earlier reported photovoltaic devices have quantum yields ranging from 0.01 to 16%, however, with generally low fill factors (<20%) and low photovoltages (<250 mV).

The dependence of open-circuit voltage and short-circuit current on the white light intensity (I_L) for one of the devices studied is shown in Figure 5. The short-circuit current (I_{sc}) has a linear dependence with light intensity. The V_{oc} value is fairly stable above a light intensity of 7 mW cm^{-2}, but decreases markedly below this intensity. This is expected, as the balance between photogeneration and recombination becomes less favorable at lower light intensities. At open-circuit conditions, all photogenerated carriers recombine within the solar cell diode. Thus, if recombination can be minimized, V_{oc} can be maximized. However, from thermodynamic considerations of the balance between radiation and generation, one finds that recombination cannot be reduced below its radiative component, yielding a basic limit for V_{oc}.[2b] Since we consider the photocurrent to be

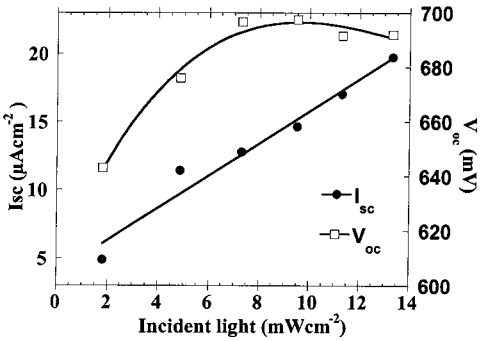

Figure 5. Short-circuit current (circles) and open-circuit voltage (squares) as a function of incident light intensity for the Au·ZOR_2POR_1/PV_3 device. The electrode was immersed in a 2.5 × 10^{-2} M aqueous solution of PV. The potential of the working electrode was set at 0 V versus SCE.

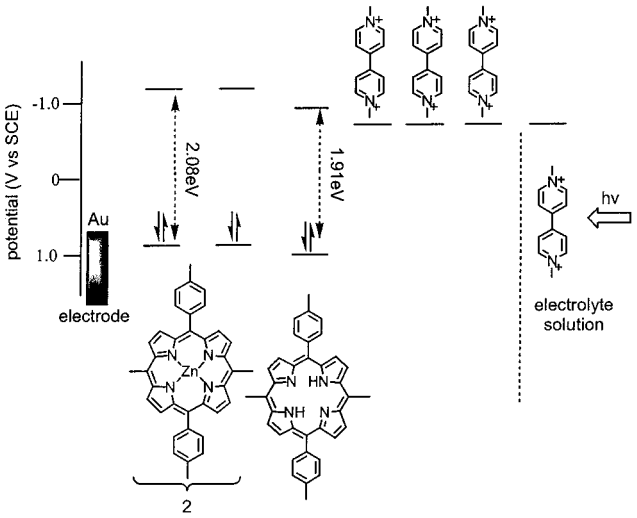

Figure 6. Schematic diagram with energies of the gold electrode modified with a Cu thiolate film of porphyrin derivatives ZOR and POR donors incorporated in a favorable cascade fashion according to their redox potentials and optical energy gap followed by a 3 layer film of ZrPV in contact with solution containing PV as an electron relay.

linearly dependent with the light intensity, this behavior is expected for a p−n hetero junction device.[23] The other devices reported here show similar intensity dependence.

The self-assembly method used here allowed us to build the multilayers with an improved arrangement of donors and acceptors. The two porphyrin donors can be organized, according to their redox potentials and optical energy gaps, in a manner that favors exciton migration to the donor−acceptor (D−A) interface, introducing a cascade arrangement that draws the holes away from the D−A interface. The energetics of this favorable arrangement is shown schematically in Figure 6. The energy levels used here correspond to those of the singlet excited states; however, a similar picture is expected for the triplet excited states as well. The thermodynamic driving force would be less for the triplet states, but the longer lifetimes for the triplets may increase the likelihood of their charge separation, prior to nonradiative relaxation. When the cascaded electrode ZOR_2-POR_1/PV_3 was under illumination and kept at 0 V versus SCE, the short circuit current density was 26 μA cm^{-2} (Figure 4). Considering the power absorbed by the porphyrin moieties (2.2

(22) (a) Memming, R. *Faraday Discuss. Chem. Soc.* **1974**, *56*, 261. (b) Watanabe, T.; Miyasaka, T.; Fujishima, A.; Honda, K. *Chem. Lett.* **1978**, 443. (c) Iriyama, K.; Mizutani, F.; Yoshiura, M. *Chem. Lett.* **1980**, 1399. (d) Fromherz, P.; Arden, W. *J. Am. Chem. Soc.* **1980**, *102*, 6211. (e) Sato, H.; Kawasaki, M.; Kasatani, K.; Higuchi, Y.; Azuma, T.; Nishiyama, Y. *J. Phys. Chem.* **1988**, *92*, 754. (g) Biesmans, G.; Auweraer, V.; Cathry, C.; Schryver, F.; Yonezawa, Y.; Sato, T. *Chem. Phys.* **1992**, *160*, 97.

(23) (a) Sze, S. *Physics of Semiconductor Devices*; Wiley: New York, 1981. (b) Greenham N.; Peng X.; Alivisatos A. *Phys. Rev. B* **1996**, *54* (24), 17628. (c) Roman, lL.; Andersson, M.; Yohannes, T.; Inganãs, O. *Adv. Mater.* **1997**, *9*, 1164

μW cm^{-2}), the quantum yield (current/absorbed photons) is calculated to be 3.5%. The calculated fill factor was 50%. The maximum power rectangle was calculated to be 7.6 μW cm^{-2}. The photoenergy conversion efficiency (output electrical watt/incident optical watt) was calculated to be 0.06%.

Some Cu metalation of the POR layer may result during the growth process, vide supra. This Cu incorporation is not expected to significantly affect the cascading process, since the POR layer will still be predominantly POR. Moreover, the copper-metalated POR would be expected to charge separate to a viologen acceptor. The loss would be in the degree of energy cascading toward the D/A interface, since the energetics of ZOR and copper-POR are similar and in the higher level of nanradiative quenching of the excited state that would be observed for copper-POR, compared to POR and ZOR. Thus, the quantum efficiencies reported above are a lower limit of what could be observed if all Cu-metalated POR impurities could be eliminated.

The increase of steady-state current and the power output observed in the favorable cascade combination ZOR_2POR_1/PV_3 compared to noncascade combinations POR_3/PV_3 and ZOR_3/PV_3, shows that careful control of the energetics in the multilayers stack can increase the photocurrent quantum yields. Figure 6 shows a simplified picture of the photoinduced electron pathway in the cascade multilayer stack. The LUMO levels of POR, ZOR, and PV are −0.91, −1.2, and −0.67 V (vs SCE), respectively. Upon illumination, excitons form in the donor layer, near the donor−acceptor interface. Electron transfer from POR to PV then occurs, forming a charge-separated state. The electron transfer from excited POR to PV is an energetically downhill pathway. Generally, it is the back electron transfer that prevents donor−acceptor (D−A) systems from achieving high yields for charge separation.[5,6] The method used here to decrease the rate of back electron transfer is to separate the hole and electron spatially by drawing the hole way from the D−A interface, using the higher energy HOMO level of ZOR. The result is an energetically favorable step to quickly generate spatially separated electrons and holes. This technique has been used widely in molecular and supramolecular systems to achieve high quantum yields of charge-separated states with long lifetimes. Here, a donor (ZOR) is incorporated that has a lower HOMO energy level than POR. HOMO levels of POR and ZOR were measured to be 1.2 and 0.88 V vs SCE, respectively. After formation of the charge-separated state at the interface between the donor and the acceptor, holes hop through an energetically downhill pathway from POR to ZOR, decreasing the back electron-transfer rate. This is clearly seen when the charge-separation quantum yield at the ZOR_2POR_1/PV_3 electrode (3.5%) is compared to that of the POR_3/PV_3 (2.4%) and ZOR_3/PV_3 (2.3%) electrodes.

Summary

Layer-by-layer lamellar growth of copper aromatic dithiolate on gold- and thiol-rich quartz substrates was demonstrated. Gold electrodes modified with zirconium viologen-bisphosphonate multilayers on top of copper porphyrin-dithiolate multilayers were photoelectroactive and could produce efficient and stable photocurrent by using visible light with quantum yields of 2−4% and fill factors of 35−60%. By arranging the zinc-porphyrin (ZOR) and the free base porphyrin (POR) donors in an energetically favorable fashion according to their redox potentials and optical energy gaps, the photoinduced charge- separation yields improved, hence improving the quantum yields and the photoelectrochemical performance of the device. Photoelectrochemical properties of these aqueous-stable electrodes make them very attractive for photocatalytic processes, such as H_2 production from water.

Scheme 2

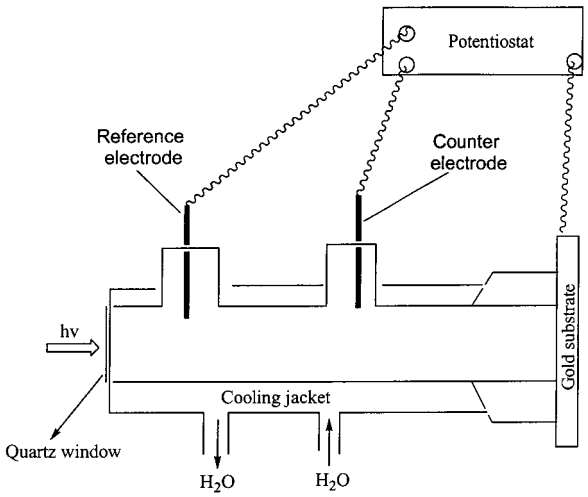

Experimental Section

General Methods. All commercially available reagents and solvents were used as received from commercial suppliers unless otherwise stated. *N*,*N*′-Bis(2-phosphonoethyl)-4,4′-bipyridinium dichloride (PV)[15] and 4-mercaptobutylphosphonic acid[24] were synthesized according to existing procedures. Ellipsometry was performed on a Rudolph Auto EL ellipsometer employing a 70 °C angle of incidence with a HeNe laser (λ = 620 nm) as the source. AFM images were obtained on a Nanoscope III Multimode microscope in the tapping mode. ^{1}H NMR spectra were obtained on a Bruker WM-250 spectrometer. Gold substrates (1000 Å of Au with 50 Å of Ti or Cr as the adhesive layer on 1 mm thick glass) were purchased from EMF Corp. Deionized water was obtained from a Millipore Milli-RX20 system.

Electrochemistry. Cyclic voltammograms (CV) were recorded on EG&G Potentiostat/Galvanostat Model 283. CV was recorded at a scan rate of 0.1 V s^{-1} with Pt wire as working and as counter electrodes and SCE as a reference electrode. CVs of the porphyrin derivatives were carried out in dichloromethane solutions with 0.1 M tetra(*n*-butyl)-ammonium hexafluorophosphate as a supporting electrolyte, while the CV of viologen (PV) was carried out in aqueous solution with $LiClO_4$ as a supporting electrolyte.

Optical Measurements. Absorption spectra were recorded on an AVIV Model 14DS-UV-Vis-IR spectrophotometer (re-engineered Cary 14). Emission spectra were recorded on a PTI QuantaMaster Model C-60SE spectrofluorometer with 928 PMT detector and corrected for detector sensitivity inhomogeneity. The absorption and emission spectra was recorded in a CH_2Cl_2 solution of the porphyrin derivatives, while aqueous solution was used in the case of PV.

Photoelectrochemical Measurements. The photocurrent measurement setup is shown in Scheme 2. The photocell was a cylindrical tube equipped with two ports and a cooling jacket. One face of the cylindrical tube is capped with a quartz window, while the opposite face is used to attach the photoelectrochemical electrode. The cooling jacket is used to remove the infrared portion of the light, preventing heating of the electrode. The two ports in the photocell were used to insert the

(24) Yang, H.; Aoki, K.; Hong, H.; Sackett, D.; Arendt, M.; Yau, S.; Bell, C.; Mallouk, T. *J. Am. Chem. Soc.* **1993**, *115*, 11855.

reference and the counter electrodes into the electrolyte solution. The gold substrate was placed facing the quartz window. The photocell was filled with a solution containing 0.025 M electron shuttle (PV) and 0.1 M $LiClO_4$ as a supporting electrolyte. The light source was a 200 W Hg/Xe Oriel Instruments arc lamp. The lamp was accommodated in a Model 60100 Oriel Instruments Photomax lamp housing. The incident light intensity was measured with a Newport 1835-C optical meter. The photocurrent measurement was based on a three-electrode configuration: the gold electrode modified with photoactive assemblies as the working electrode, a reference (SCE), and an inert counter electrode (Pt coil).

Synthesis and Thin-Film Preparation. The preparation of the POR and ZOR derivatives was carried out by standard procedures. The detailed syntheses and characterization of these compounds are given the Supporting Information.

Preparation of Thin Films. Thin films of zirconium bisphosphonate were grown using methodology developed by Mallouk and Katz.[15] Thin films of Cu dithiolate were grown using a similar method developed by Ulman and co-workers.[17] All deposition solutions were filtered through a 0.45 μL syringe filter. Gold substrates were cleaned by oxidation with a UV/ozone cleaner, washed with deionized water, and then blown dry. Monolayers of POR or ZOR on Au were prepared by placing the freshly cleaned Au slides in a degassed dilute solution of the dithiol (1 mmol in dry THF) for 15 h under N_2, followed by thorough rinsing with THF. This thiol-enriched surface was used to construct Cu-thiolate multilayers by alternate treatments in a dilute solution of $Cu(OAc)_2$ (20 mmol in absolute EtOH) for 15 min and then the dithiol solution for 20 min. To build multilayers of Zr bisphosphonate on top of a Cu-thiolate film, the thiol-terminated surface was treated with $Cu(OAc)_2$, followed by a surface treatment in mercaptobutylphosphonic acid for 30 min followed by $ZrOCl_2$ solution (15 min), and then the Zr bisphosphonate multilayers were grown by alternative treatment of the $ZrOCl_2$ (15 min) and viologen-bisphosphonates (20 min) at 70 °C.

Acknowledgment. This work was supported by the Global Photonic Energy Corporation, the Airforce Office of Scientific Research through Multidisciplinary University Research Institution (MURI) program, and the National Science Foundation.

Supporting Information Available: The syntheses and characterization data for the POR and ZOR derivatives (PDF). This material is available free of charge via the Internet at http://pubs.acs.org.

JA011700M